Three-Dimensional Concentration Mapping of Organic Blends

John D. Roehling, K. Joost Batenburg, F. Benjamin Swain, Adam J. Moulé, and Ilke Arslan**

The three-dimensional morphology of mixed organic layers are quantitatively measured using high-angle annular dark-field scanning transmission electron microscopy (HAADF-STEM) with electron tomography for the first time. The mixed organic layers used for organic photovoltaic applications have not been previously imaged using STEM tomography as there is insufficient contrast between donor and acceptor components. Contrast is generated by substituting fullerenes with *endohedral* fullerenes that contain a Lu_3N cluster within the fullerene cage. The high contrast and signal-to-noise ratio, in combination with use of the discrete algebraic reconstruction technique (DART), allows generation of the most detailed and accurate three-dimensional map of BHJ morphology to date. From the STEM-tomography reconstructions it is determined that three distinct material phases are present within the BHJs. By observing changes to morphology and mixing ratio during thermal and solvent annealing, the effects of mutual solubility and fullerene crystallization on morphology and long term stability are determined. This material/technique combination shows itself as a powerful tool for examining morphology in detail and allows for observation of nanoscopic changes in local concentration.

1. Introduction

Self-assembled mixtures of electron donor polymers and acceptor fullerenes have been studied for use in organic photovoltaic (OPV) devices for nearly a decade. It has been exhaustively shown that device efficiency is extremely sensitive to the morphology of the mixed bulk–heterojunction (BHJ) layer.[1–5] The morphology is, in turn, affected by processing conditions and can continue to develop throughout the lifetime of the OPV device.[6–8] It is a tacit assumption of OPV device modeling[9,10] and theories of operation[11,12] that the function of an OPV device could be completely understood if a three-dimensional (3D) map of material location could be accurately measured. Until now, it has not been possible to obtain a detailed 3D BHJ composition map due to most imaging techniques lacking simultaneous high spatial resolution and high contrast between components. Electron tomography (ET) is one of the few 3D techniques capable of high spatial resolution, at 1 nm.[13] Several studies have produced 3D images that map out particular components of BHJ films using ET and bright-field transmission electron microscopy (TEM), or energy-filtered TEM (EFTEM).[14–19] These studies resolved the crystalline, fibril-like structures present in poly(3-hexylthiophene)/phenyl-C61-butyric acid methyl ester (P3HT/PCBM) blend BHJs, and contributed much to the understanding of BHJ morphology. However, a complete composition map of the BHJ layer could not be obtained due to the limitations of the techniques used. Bright-field TEM suffers from the need to defocus the image in order to generate contrast between the materials, which can change the apparent size of features, as well as cause contrast reversals. This can lead to artifacts in the reconstruction[18] and erroneous quantitative analysis. EFTEM overcomes the problems of low contrast and the need to defocus by generating contrast using differences in the energy-loss spectra of the pure components.[18,20] While effective, EFTEM suffers from a low signal-to-noise ratio because of the relatively low percentage of inelastically scattered electrons.

To overcome these limitations, we used a combination of high-angle annular dark-field scanning TEM (HAADF-STEM) tomography and BHJs consisting of P3HT and endohedral fullerenes.[21,22] HAADF-STEM tomography has been successfully applied to organic/inorganic hybrid systems,[23] but not to purely organic blends. In HAADF-STEM, the image intensity depends approximately on the square of the atomic number.[24] Since the endohedral fullerenes used here contain Lu_3N

J. D. Roehling, Prof. A. J. Moulé
Chemical Engineering and Materials Science
University of California
Davis, One Shields Ave. Davis, CA 95616, USA
E-mail: amoule@ucdavis.edu
Prof. K. J. Batenburg
Centrum Wiskunde & Informatica
P.O. Box 94079, NL-1090 GB Amsterdam, Netherlands
Prof. K. J. Batenburg
Vision Lab
University of Antwerp
Universiteitsplein 1, Building N, 2610 Wilrijk, Antwerp, Belgium
Dr. F. B. Swain
Luna Innovations, Inc., 521 Bridge St. Danville, VA 24541-1405, USA
Dr. I. Arslan
Pacific Northwest National Laboratory
PO Box 999, Richland, WA 99352, USA
E-mail: ilke.arslan@pnnl.gov

DOI: 10.1002/adfm.201202190

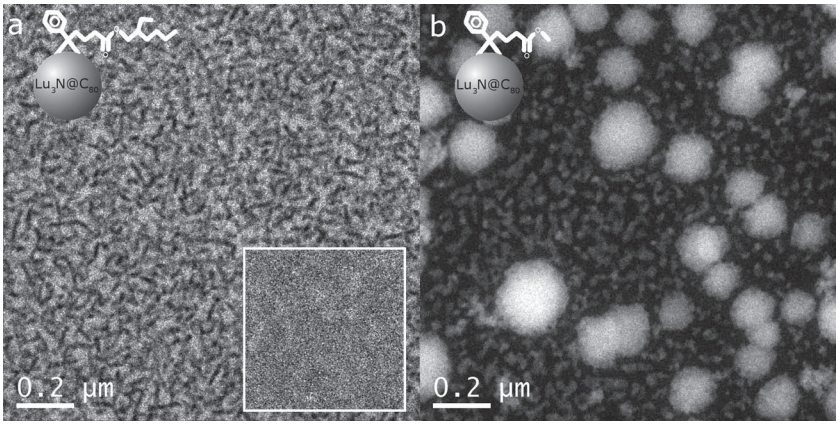

Figure 1. Comparison of STEM images of annealed BHJs. Shown are STEM images of a) P3HT/Lu-PCBEH BHJ and b) P3HT/Lu-PCBM BHJ. Inset (top): Structure of the endohedral fullerene used in the film, respectively. Inset in (a): an image of a P3HT/PCBM BHJ taken with 4× the beam current at the same magnification as in (a) and (b). All displayed images were low-pass filtered to clearly demonstrate the important features.

clusters, the contrast is drastically increased between the polymer and fullerene components. The image intensity increases monotonically with specimen thickness (an ET requirement), and also with increasing fullerene composition (increased fullerene content will appear brighter, as more electrons will be scattered for the same sample thickness). Exploiting this relationship, in conjunction with a discrete algebraic reconstruction technique (DART), we determined and quantified the existence of a distinct mixed phase that exists between the P3HT- and fullerene-rich domains. It has been demonstrated that DART strongly reduces reconstruction artifacts and leads to a quantitatively reliable segmentation.[25–27] Conventionally, a tomography dataset is first reconstructed, then segmented (assigning dark or bright domains to different materials). Segmentation is often done manually and has no constraints requiring the segmented reconstruction to match the original images. This can lead to erroneous quantification. DART, however, automatically segments the reconstructions into different materials (by assigning a constant gray-level to each material) while simultaneously constraining the reconstruction to closely represent the original images (i.e., minimize projection error).[25–27] Because we use a physically relevant 3D model and there is close agreement with the original images, we are able to accurately determine the volumetric quantity, composition, and position of each phase, thereby effectively mapping a three-dimensional material concentration profile.

Numerous recent studies have pointed to the partial miscibility of fullerene derivatives in a polymer matrix.[7,8,28–36] These studies suggest that the miscible regions consist of amorphous polymer chains intermixed with amorphous fullerene. The published composition of this mixed phase in P3HT ranges from ≈10 to ≈35% volume C_{60}-PCBM. The variability has been attributed to the different molecular weight, regioregularity, and polydispersity of commercially available P3HT, as well to fullerene crystallinity.[8] In this work, we studied two different endohedral fullerene/P3HT BHJs, $Lu_3N@C_{80}$-PCBM (Lu-PCBM) and $Lu_3N@C_{80}$-PCBEH (ethyl-hexyl, Lu-PCBEH). $Lu_3N@C_{80}$ fullerene derivatives have been used in OPV devices with power conversion efficiencies (PCE) greater than 4%.[21,22,37,38] The mutual miscibility of Lu-PCBEH/P3HT is expected to be higher than that of Lu-PCBM/P3HT due to the ethyl-hexyl side-chain. We expect that the miscibility of Lu-PCBEH is similar to C_{60}-PCBM because transient absorption measurements of BHJs show similar separated charge recombination rates over a wide temperature and composition range.[39] Fabricated devices also show similar short-circuit current and filling factors[21,22] and our tomography measurements show approximately 30 vol% Lu-PCBEH is present when intermixed with amorphous P3HT.

2. Results and Discussion

2.1. Resolving the Mixed Phase in 3D

To examine the evolution of morphology within a BHJ, we performed tomography on as-cast, thermally-annealed, (TA)[40] and solvent-annealed (SA)[3,41,42] BHJs (see the Experimental Section). We prepared BHJs of each fullerene by closely matching the volume percent ratios to a 1:1 P3HT/PCBM by weight device (≈42 vol% fullerene, C_{80} has a larger volume than C_{60}). This should mimic the morphology of an optimized BHJ (as we will demonstrate).[3,40]

Figure 1 demonstrates the large contrast between components that the endohedral fullerenes generate in 2D-STEM images. Shown are TA BHJs of both endohedral fullerenes studied. For reference, a conventional P3HT/PCBM BHJ is shown in the inset of Figure 1a, displaying no discernible contrast between polymer and fullerene components. All three images were taken at identical magnification, but the inset was acquired at four times the beam current of the others, in attempt to increase the signal-to-noise ratio and the visible contrast between components. The fullerene-rich domains (bright) can clearly be distinguished from the polymer domains (dark) in the endohedral fullerene BHJs, but are nearly impossible to distinguish in the PCBM BHJ, despite the increased signal-to-noise ratio.

By performing many reconstructions using different sets of gray-levels, we determined a two-phase model was insufficient to represent BHJs, and at least three phases were necessary to accurately match the original images (see the Supporting Information for details). The phases present are a pure P3HT-phase, a fullerene-rich phase, and a mixed phase. Pure P3HT is assumed because fullerenes cannot intercalate into crystalline domains of P3HT and in high magnification studies, no fullerene was observed in this phase.[31,43] Similar studies of BHJs showing three-phase maps have been performed previously, using electron energy-loss measurements (EFTEM), and atomic force microscope (AFM) measurements,[30,44] but this is the first time, to our knowledge, that three-phase maps have been obtained in 3D. **Figure 2** shows volume reconstructions of each phase of the as-cast, TA, and SA BHJs for the Lu-PCBEH.

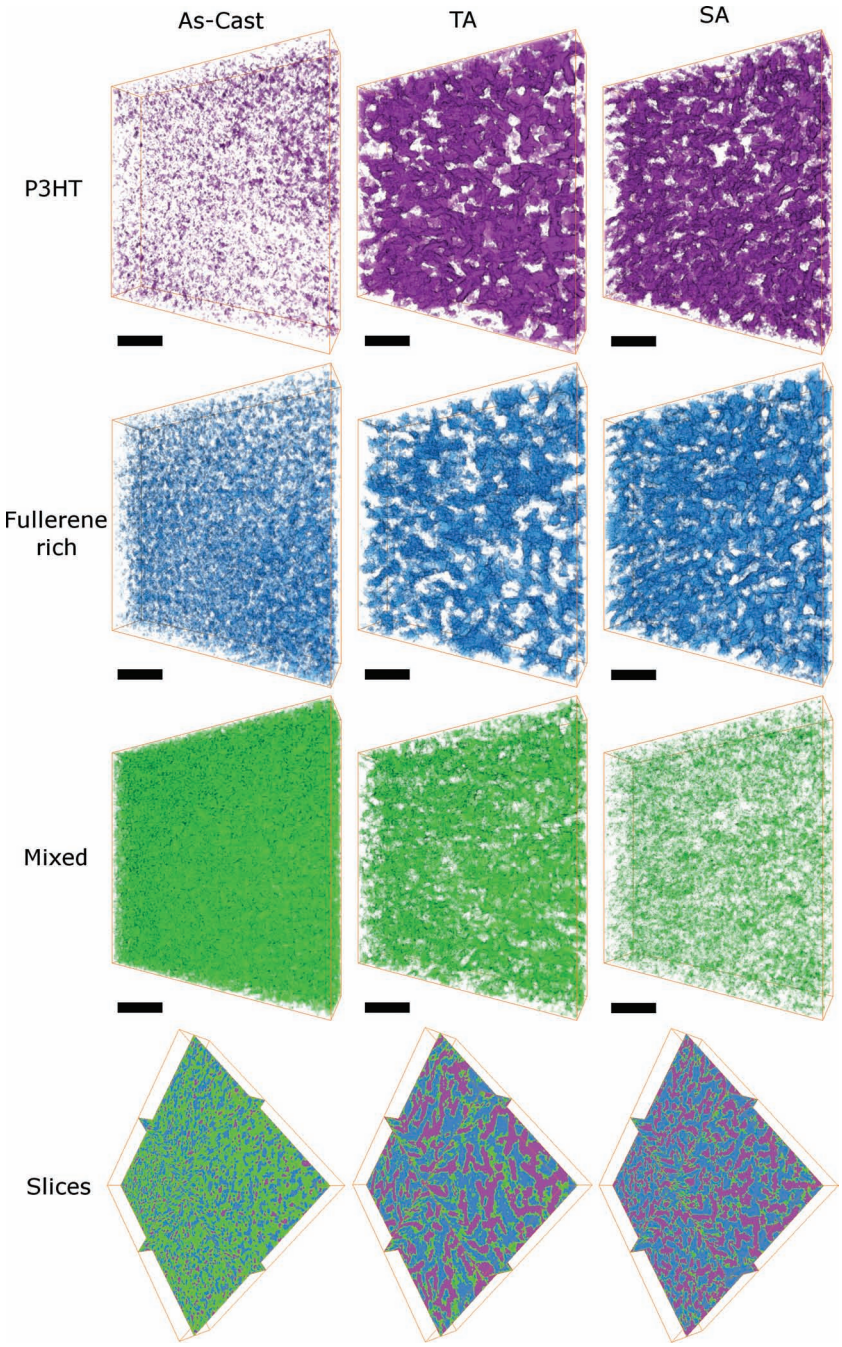

Figure 2. Reconstructions of Lu-PCBEH BHJ films. Each phase of the as-cast, TA, and SA Lu-PCBM BHJ films are shown separately, volume rendered with a 10% opacity. The P3HT phase is shown in purple, the fullerene-rich phase in blue, and the mixed phase in green. The scale bars are 100 nm and every film's dimensions are 500 nm × 500 nm × 95 nm. The last row shows slices of the reconstruction volume through all three planes (*xy*, *yz*, *xz*) in each film to illustrate how the different phases fit together. Shown are the as-cast (left), TA (middle), and SA (right) films. These are displayed with a 135° counter-clockwise rotation from the volume reconstructions.

Figure 3 shows the volume reconstructions for the as-cast and TA Lu-PCBM BHJs. The SA Lu-PCBM BHJ film was not reconstructed due to large-scale, and near complete phase separation of the components. Reconstructing this film would yield no new information about the morphology beyond what could be seen by 2D images. The voxel sizes of the reconstructions are 1.4 × 1.4 × 1.4 nm, with the achieved resolution being somewhat larger, 2–3 nm. This is due to a smoothing step in the reconstruction technique and possible image misalignments in the tilt-series. Regardless, these reconstructions are still the most accurate representations of a BHJ published to date.

We calculated the composition of each phase by a simple mass balance, assuming calculated densities of the pure components and $\Delta V_{mix} = 0$ (1.05 g/cm^3 for P3HT, 1.77 g/cm^3 for Lu-PCBM and 1.87 g/cm^3 for Lu-PCBEH, see the Supporting Information). The fullerene-rich phase and mixed phase were also assumed to have a concentration ratio between them which was based on their intensity (gray-level) in the reconstruction. It must be noted here that the calculated compositions are purely a result of obtaining the best reconstruction fit using a three phase model. **Table 1** summarizes the volume percent and composition of each phase in the examined samples. These values were obtained by averaging over volumes much larger than those shown in Figure 2 and Figure 3, ≈1.1 µm across.

There are countless features in these reconstructions, most of which cannot be addressed in this first article. Some immediate features that can be seen in Figure 2, is that the domains of the P3HT phase have the size and shape of crystalline P3HT fibrils which have been observed in P3HT/PCBM BHJ films.[14–17] This suggests that the domain sizes in these endohedral films are similar in size to those in conventional BHJs. It must be mentioned that although the morphology observed in these films is similar an OPV device, it is not fully representative. A recent study by Mauger et al. has shown that, when capped with a metal electrode (as most devices measured for performance are), vertical segregation of the fullerene to the electrodes occurs upon heating.[45] The films here were not fabricated with a top metal electrode, and so the vertical concentration profile is different. Work is currently being done on being able to image capped films, but this is the subject of a future publication.

Despite not fully representing OPV device morphology, measurements of these films did allow us to examine many of the effects mixing has on BHJ morphology. Several general trends observed in Figure 2 and Figure 3 suggest that this technique provides accurate three-phase mapping. First, both TA and SA induce "demixing" of the mixed phase in both fullerene BHJs (this is due to both P3HT crystallization and fullerene

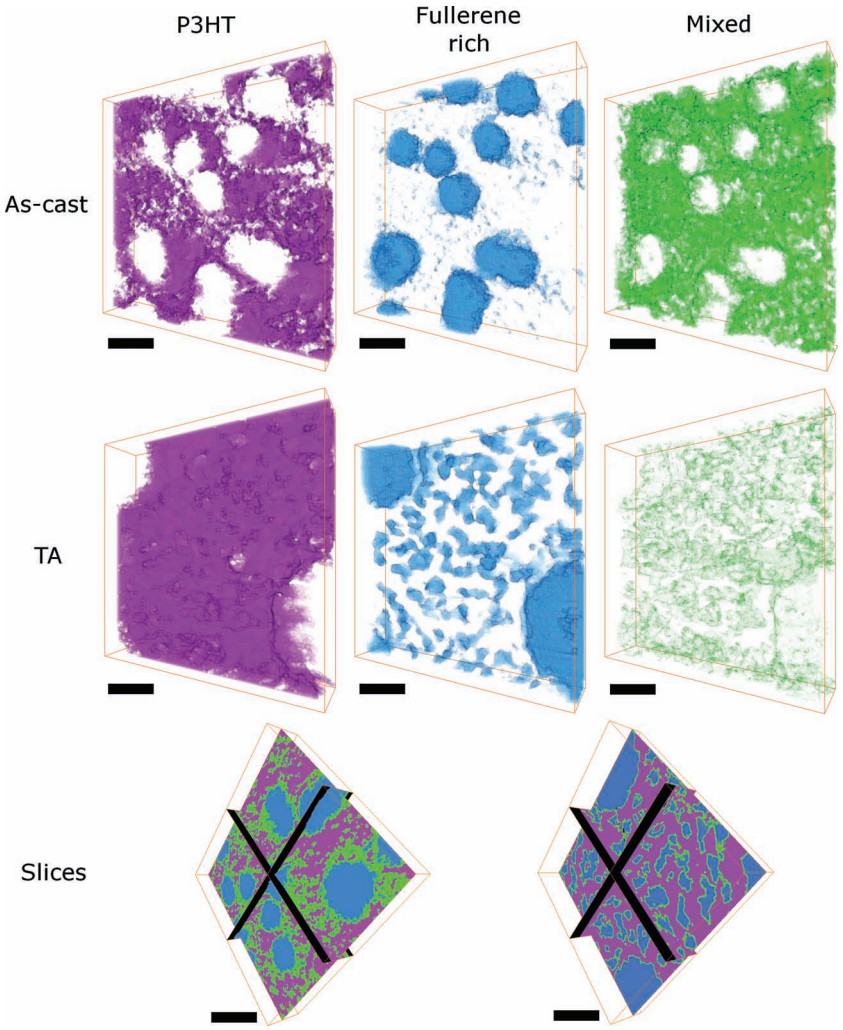

Figure 3. Reconstructions of Lu-PCBM BHJ films. Each phase of the as-cast and TA Lu-PCBM BHJ films are shown separately, volume rendered with a 10% opacity. The SA film was not reconstructed due to large-scale phase separation. The P3HT phase is shown in purple, the fullerene-rich phase in blue, and the mixed phase in green; black is vacuum. The scale bars are 100 nm and every film's dimensions are 500 nm × 500 nm × 95 nm. The two lower panels show slices of the reconstruction volume through all three planes (*xy*, *yz*, *xz*) in the as-cast (left) and TA (right) film to illustrate how the different phases fit together. These are displayed with a 135° counter-clockwise rotation from the volume reconstructions.

Table 1. Total volume percent of each component in each phase (shown in pie graphs) and the volume percent fullerene contained in each phase of all the endohedral fullerene BHJ films studied.

	Lu-PCBEH			Lu-PCBM		
% Vol Fullerene Mixed Phase	30±7	49±4	31±4	31±7	55±7	~0
% Vol Fullerene Fullerene Rich Phase	78±7	90±4	94±4	95±7	96±7	~100

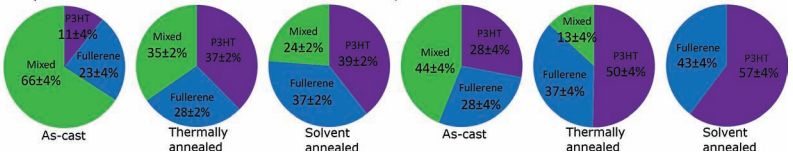

Errors are given by the maximum effect that varying the gray levels has on the composition while still minimizing projection error and maintaining mass balance. Errors represent 95% confidence intervals.

aggregation, as will be demonstrated). Second, the mixed phase is always found at the interface between the P3HT- and fullerene-rich phases. Lastly, there is reduced mixed phase content with a less soluble fullerene and the composition changes with temperature.

A principal theme in the literature is that P3HT/PCBM BHJ efficiency is increased by TA or SA.[42,46] Figure 2 shows an increased number of charge percolation pathways in the annealed BHJs. Holes and electrons can be transported through the pure P3HT- and fullerene-rich phases, respectively, as the connectivity to the electrodes in these domains is very high. In the as-cast sample, there are nearly no percolation pathways through pure P3HT domains, whereas there are numerous pathways through fullerene-rich domains. Therefore, in as-cast devices, holes must be transported through the mixed phase in which the P3HT assumes an amorphous form. Here, hole mobility is reduced and the band gap is increased. The reconstructions corroborate previous work showing that electron mobility in as-cast devices is similar to that of annealed devices, whereas the hole-mobility increases several orders of magnitude after annealing, resulting in balanced mobilities.[47,48] Our data shows that this is most likely due to the formation of phase-separated, charge percolation pathways.

2.2. Mixed Phase Affects Local Morphology

The evolving morphology not only reveals changes in the component rich phases, but also reveals the effects of the mixed phase. These effects can be seen by comparing the Lu-PCBEH samples to the Lu-PCBM samples. Because Lu-PCBEH has a higher mutual solubility with P3HT, larger volumes of the mixed phase are present in both the as-cast film (66% rather than 44%) and the annealed films (35% and 24% rather than 13% and 0%), when compared to the Lu-PCBM. Visual inspection of the reconstructions makes obvious that the domain sizes are much smaller and more continuous for the pure phases in the Lu-PCBEH samples. A smaller amount of mixed phase present seems to affect the formation of larger domains of pure phases. This suggests that the mixed phase is critical for the formation of a "desirable" BHJ morphology with the optimum length-scales.

The miscibility of the components seems to have direct effect on the volume and composition of the mixed phase, as is expected. The expected crystallinity of P3HT in annealed

BHJs is ≈50%.[2,49,50] However, in the TA Lu-PCBM film the P3HT- phase includes ≈86% of the total P3HT, and there are no well defined fibrils of P3HT observed in the rendered volume (Figure 3). This suggests that there are many domains of pure amorphous P3HT in this film. Treat *et al.* showed, however, that PCBM mixes readily with amorphous domains of P3HT.[29] It seems that due to the lower miscibility of Lu-PCBM compared to Lu-PCBEH or PCBM, it is more energetically favorable for Lu-PCBM to aggregate with itself, rather than remain in the P3HT matrix, even though amorphous P3HT is present. By comparison, in the TA Lu-PCBEH samples, the P3HT phase contains mostly crystalline P3HT fibrils (the P3HT phase contains ≈63% of the total P3HT), and the remaining amorphous P3HT readily mixes with the fullerene. In other words, higher miscibility leads to a more persistent mixed phase, seen as an increase in the mixed phase volume.

Comparing the annealed samples in more detail allows us to better define the exact role of the mixed phase. For both acceptors, the SA sample has less mixed phase volume and reduced fullerene content in the mixed phase compared to the TA samples. If we assume the equilibrium morphology requires phase separation into only two phases, as is seen in the Lu-PCBM SA sample, then our data suggest that SA facilitates morphological relaxation, while TA leaves the sample kinetically frozen. Other studies of long-term thermal annealing show morphologies similar to that in the SA Lu-PCBM sample (very large fullerene crystals present and a fullerene depleted P3HT region).[31] As such, we assume that SA facilitates the same degree of relaxation (quasi-equilibration) in both films. With this assumption in mind, this data shows that the mixed phase continues to persist at ≈25% of the total volume in the Lu-PCBEH BHJ after equilibration.

The composition of the mixed phase is 30 vol% fullerene in both the as-cast sample and SA sample but is 43 vol% in the TA sample for Lu-PCBEH. The difference in mixing ratio is due to the sample's fabrication history. The mutual solubility between P3HT and Lu-PCBEH is higher at 150 °C than at room temperature.[8] The TA sample was kept at 150 °C for 5 min and then rapidly quenched to room temperature, freezing in the more miscible composition and morphology. The same effect is seen in the TA Lu-PCBM sample, the mixed phase contains more fullerene than in the as-cast sample.

The different effects that SA and TA have on the mixed phase are best demonstrated in the poorly-miscible Lu-PCBM samples. The SA sample has no detectable mixed phase, which leads us to conclude that there is very low miscibility between P3HT and Lu-PCBM at room temperature.[28,31] In the TA sample, the large fullerene aggregates attest to the poor solubility of Lu-PCBM in P3HT. But in the same image there are well-defined nanometer-sized domains of Lu-PCBM that appear to be ideal for an OPV layer. These domains are formed at 150 °C, a temperature for which a mixed polymer/fullerene phase is stable (13 vol%). Previous reports claim that both P3HT and fullerene crystallization drive phase separation.[8,51,52] We agree. But the mixed phase seems to be essential to mediate the phase-separation and seems to help minimize large aggregate formation which are ineffective for efficient OPV operation.

Despite this evidence, the question remains: If some small amount of miscibility exists and the mixed phase allows nanoscale morphology to persist, then why did the SA Lu-PCBM sample completely phase-separate? Until this point in the article, we treated the BHJ layer as a three-phase mixture with the phases being pure P3HT fibrils, a P3HT-rich mixture of amorphous P3HT with amorphous fullerene (referred to as the mixed phase), and a fullerene-rich mixture of amorphous P3HT with amorphous fullerene (the fullerene-rich phase). However, Collins et al.,[8,28] recently showed that fullerene (PCBM) crystallization is major driving force for large-scale phase separation in BHJ blends. This result suggests that a fourth phase consisting of crystalline fullerene should exist in BHJ mixtures. We note, however, that the difference is not resolvable using this technique. The concentrations are too similar which results in any crystalline-fullerene domains being displayed as part of the fullerene-rich phase. This may, to some extent, explain why the vol% of fullerene in the fullerene-rich phase is processing-dependent (see Table 1). We did observe some crystallinity in the large aggregates of the TA Lu-PCBM samples, but the vast majority were amorphous (Supporting Information Figure S2). However, from the TA and SA data, it seems that fullerene crystallization depletes the mixed phase of fullerene, reducing or eliminating it, which destabilizes the morphology.

We examine this by comparing SA samples. **Figure 4** shows 2D-STEM images of both SA samples at low magnification. The bright blobs are agglomerates of fullerene, the lighter gray is the carbon support, and the darker areas are the BHJ film. In Figure 4a, the nanoscale morphology of the Lu-PCBEH sample remains preserved (Figure 2), but some fullerene aggregation is present. The Lu-PCBM sample, however (Figure 4b), shows

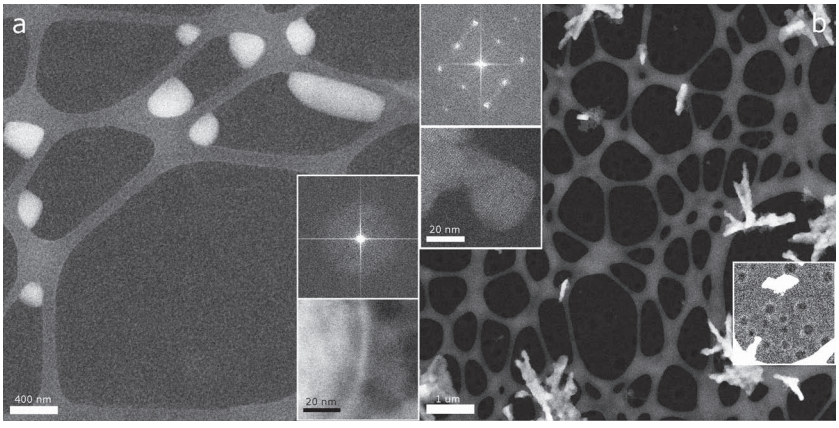

Figure 4. Low magnification STEM images of SA-BHJs. The images show fullerene aggregation and crystallization in the a) Lu-PCBEH and b) Lu-PCBM BHJs, respectively. The images are at separate magnification to illustrate separate features. Inset in (a) and (b) are high magnification images of the agglomerates (bottom) and the fast Fourier transform of the high-magnification images (top) showing the periodicity of the fullerene agglomerates. The lower right box in (b) is displayed with increased contrast and brightness to allow visualization of the hole-like features present in the film.

nearly complete phase separation with large fullerene crystals, several micrometers across, present (this occurred throughout the entire film, see Supporting Information Figure S1). Higher magnification studies showed no discernible fullerene left in the film, outside the large crystals (images not shown), which led us to assign the compositions of the SA Lu-PCBM sample to be pure phases. The inset of Figure 4b shows a high-magnification image of one of the dendritically grown fullerene crystals,[53] along with the fast Fourier transform (FFT) of the image, demonstrating its crystallinity (see the Supporting Information for more details).

Some large fullerene aggregates (Supporting Information Figure S1) are observed in the SA Lu-PCBEH sample, but fullerene crystallization did not occur. The upper inset of Figure 4a shows the FFT of a representative Lu-PCBEH agglomerate (lower inset) displaying an amorphous ring. The crystallization is suppressed here, likely by the ethyl-hexyl side chain, as well as by increased miscibility. Despite this, the formation of fullerene-rich domains still occurs. We need to briefly return to the role of the mixed phase to fully understand the effect of fullerene crystallization. There are two possibilities for the formation of the fullerene-rich phase. Firstly, as Kozub *et al*. suggested,[18] crystallization of the P3HT could be driving excess fullerene into the mixed phase, pushing it past the solubility limit, causing the formation of the fullerene-rich phase. But, this should cause the fullerene-rich phase to be directly adjacent to the P3HT phase, which is not observed. The other possibility (which our data supports) is that the fullerene-rich phase grows from direct aggregation of the fullerene, in addition to P3HT crystallization. Here, both P3HT and fullerene-rich domains deplete the mixed phase of material, but once enough fullerene leaves the mixed phase to reach the solubility limit, fullerene aggregation ceases (or becomes very, very slow). It is no longer more energetically favorable for the fullerene to aggregate, so it remains in the mixed phase. Aggregation should also leave a depleted region (the mixed phase) surrounding the fullerene-rich phase, which is indeed observed in the reconstructions. Lastly, the presence of large fullerene aggregates themselves suggest fullerene aggregation is driving phase segregation. P3HT crystallization alone will likely not cause enough local build up of fullerene for large aggregates to form (Supporting Information Figure S1).

Altogether, the mixed phase seems to mediate phase separation by only allowing the fullerene-rich phase to grow to a certain extent. Additionally, if the solubility limit is higher, more mixed phase should be present because less fullerene can aggregate into fullerene-rich domains. Indeed, this was observed in the TA and SA Lu-PCBEH samples. The TA sample, containing a higher concentration of fullerene in the mixed phase (the TA sample was frozen into a higher solubility state when it was quenched from high temperature) also contained a larger volume of mixed phase. Conversely, lower solubility should contain less mixed phase, and this was observed in the TA Lu-PCBM sample.

From the SA samples, we see that fullerene crystallization seems to reduce amount of the mixed phase present, which allows for large-scale phase separation. The low energy fullerene crystals seem to draw fullerene from the mixed phase, despite some solubility being present. However, in the non-crystallizing case of Lu-PCBEH, the growing amorphous fullerene domains cannot easily withdraw fullerene from the mixed phase past the solubility limit, explaining why the Lu-PCBEH mixed phase persists after SA and the Lu-PCBM mixed phase does not. This illustrates the importance of having a persistent mixed phase to maintain the morphology of a BHJ. Fullerene crystallization seems to reduce the persistence of the mixed phase, which drives large-scale phase separation.

The small aggregates visible in Figure 4a, occurred after the film was placed onto the TEM grid. This can be deduced because there were no aggregates of this size anywhere in the film, except for in areas immediately adjacent to the carbon support. If aggregation occurred before placing the film on the carbon support, then aggregates should be seen in other locations. They were not. Additionally, aggregation occurred mostly in areas with high curvature on the carbon grid. This suggests that some aggregation is caused by an interaction with the underlying substrate and that surface energy has an effect on aggregation. The aggregation is surprising due to the fact that the film was at room temperature upon deposition on the carbon grid. However, we have shown previously that despite drying the films in vacuum, residual solvent remains trapped in the film, lending the fullerene high mobility in the P3HT matrix.[54] This is likely what allowed for the growth of the small aggregates. Trapped solvent must have also allowed the mixed phase to equilibrate to the room temperature composition, despite having been heated to a more miscible state. We estimate greater than 95% of the film did not have any large aggregates and the morphology looked similar to the TA film, as shown in Figure 2, demonstrating the highly stable morphology of the Lu-PCBEH BHJ.

Increasing the component miscibility seems to be one way to assist in inhibiting fullerene crystallization. In all the BHJs, except the SA Lu-PCBM, both the mixed and fullerene-rich phases are shown to consist partially of P3HT. Kozub *et al*. also demonstrated that P3HT exists throughout the entire device.[20] In Figure 4b, the lower right inset shows dark, round features corresponding to thin regions of the film. The period and size of these regions correlates exactly to the period and size of fullerene aggregates in the as-cast sample. We conclude that these regions are where large fullerene aggregates used to reside, formed by the collapse of the intermixed P3HT upon the exodus of the fullerene. This clearly demonstrates that the fullerene-rich phase is not pure, but consists partially of some intermixed P3HT, confirming our composition assignments. The widespread lack of fullerene crystallinity in the TA Lu-PCBM sample clearly demonstrates that the presence of P3HT can inhibit crystallization of the fullerene: just as the presence of the fullerene can inhibit crystallization of the P3HT.[20,36,55] It cannot completely prevent it, however, as Figure 4b and Supporting Information Figure S2 demonstrate. A recent study of non-crystallizing fullerenes in BHJs gives strong evidence that preventing fullerene crystallization can prevent large scale phase separation.[56] We recommend that new functionalized fullerenes be synthesized that induce miscibility but prevent crystallization (PCBEH for example). This is one possible route to stabilizing the morphology of polymer-fullerene blends.

3. Conclusions

We have shown that a three-phase model is needed to accurately describe the morphology of partially miscible P3HT/

endohedral fullerene BHJs. Our results agree with many previous studies involving the mixing and morphological evolution of P3HT/PCBM BHJs. In addition to being consistent with other studies, our results show that in these films a mixed phase seems to be necessary to mediate the phase separation of components, and to maintain the optimum morphology of a BHJ blend. Two major factors affecting mixed phase persistence were identified: the overall component miscibility and the presence of fullerene crystallization. Increased miscibility increases the mixed phase volume and fullerene content, whereas fullerene crystallization, by depletion of the mixed phase, eventually leads to large-scale phase separation. Therefore, the suppression of fullerene crystallization and inducing component miscibility seem to be possible routes to stabilizing the morphology of polymer-fullerene blends. Through the use of Lu_3N-containing endohedral fullerenes and ET, we have demonstrated an effective method for generating detailed morphology maps. The new morphological information can be effectively correlated to charge mobilities, spectroscopic measurements, and device characteristics in ways which were not previously possible with other techniques.

4. Experimental Section

Sample Preparation: Samples were prepared by first cleaning glass slides by wiping down with chloroform, then ultrasonicating in acetone, detergent and then deionized water for 15 min each. Next, poly(3,4-ethylenedioxythiophene):poly(styrenesulfonate) (PEDOT:PSS) was spin-cast onto the substrate (in air) at 2500 RPM for 60 s. This was then placed on a hotplate for 5 min at 110 °C and subsequently transferred into a nitrogen glovebox. A solution of P3HT/fullerene (65 kDa from Plextronics) was spin-cast onto the substrate at 60 °C. The solutions were 10:13 P3HT/Lu-PCBEH by weight (≈20 mg mL^{-1}) and 4:5 P3HT/Lu-PCBM by weight (≈10 mg mL^{-1} due to lower solubility). The prepared films were then either annealed at 150 °C for 5 min and then transferred onto a TEM lacey carbon grid or transferred directly onto a lacey carbon grid. This was done by floating off the film in deionized water and scooping up a flake with the TEM grid. For the SA films, as-cast films were placed on a hot plate at 150 °C under an inverted Petri dish along with a small dish of 1,2-ortho-dichlorobenze for 2 h. Afterwards, the film was dried for several days in vacuum before transferring it to a TEM grid. The film thicknesses were ≈100 nm and ≈80 nm for the Lu-PCBEH and Lu-PCBM films, respectively.

Imaging and Analysis: All STEM images used for the ET reconstructions were taken with an JEOL 2100F at 200 kV. Tilt series were taken using dynamic focus via a STEM tomography plugin for DigitalMicrograph (Gatan). Images were taken at one degree intervals from a minimum of +65 to –65 degrees. They were aligned manually using IMOD and 3D reconstructions were done using custom code in MATLAB. Volumes were visualized using Avizo 6.0 (VSG).

Supporting Information

Supporting Information is available from the Wiley Online Library or from the author.

Acknowledgements

J.D.R. and A.J.M. wrote the manuscript, J.D.R. performed the STEM imaging, 3D reconstructions and analysis. K.J.B. developed the DART algorithm assisted with its implementation. F.B.S. synthesized the endohedral fullerenes used in the study. I.A. supervised the STEM tomography imaging, reconstructions, and analysis and A.J.M. supervised the sample preparation and materials science interpretation and calculations. We thank Luna Innovations, Inc. for donating the endohedral fullerenes used in this study and Plextronics for the P3HT. We also thank Wim van Aarle for coding the DART algorithm and assisting with its implementation. We gratefully acknowledge Nigel Browning and the UC Lab Fee for financially supporting the work and The National Science Foundation Energy for Sustainability Program, Award No. 0933435. This research was supported in part by the Laboratory Directed Research & Development program at PNNL. The Pacific Northwest National Laboratory is operated by Battelle for the US Department of Energy under contract DE-AC05-76RL01830. K.J.B. was supported by the Netherlands Organisation for Scientific Research (NWO), programme 639.072.005.

Received: August 3, 2012
Revised: September 27, 2012
Published online: November 19, 2012

[1] D. Chirvase, J. Parisi, J. C. Hummelen, V. Dyakonov, *Nanotechnology* **2004**, *15*, 1317.
[2] A. J. Moulé, K. Meerholz, *Adv. Mater.* **2008**, *20*, 240.
[3] G. Li, V. Shrotriya, J. Huang, Y. Yao, T. Moriarty, K. Emery, Y. Yang, *Nat. Mater.* **2005**, *4*, 864.
[4] M. Reyes-Reyes, K. Kim, D. L. Carroll, *Appl. Phys. Lett.* **2005**, *87*, 083506.
[5] W. L. Ma, C. Y. Yang, X. Gong, K. Lee, A. J. Heeger, *Adv. Funct. Mater.* **2005**, *15*, 1617.
[6] D. M. Huang, S. A. Mauger, S. Friedrich, S. J. George, D. Dumitriu-LaGrange, S. Yoon, A. J. Moulé, *Adv. Funct. Mater.* **2011**, *21*, 1657.
[7] C. Müller, J. Bergqvist, K. Vandewal, K. Tvingstedt, A. S. Anselmo, R. Magnusson, M. I. Alonso, E. Moons, H. Arwin, M. Campoy-Quiles, O. Inganas, *J. Mater. Chem.* **2011**, *21*, 10676.
[8] B. A. Collins, J. R. Tumbleston, H. Ade, *J. Phys. Chem. Lett.* **2011**, *2*, 3135.
[9] K. Maturova, S. S. van Bavel, M. M. Wienk, R. A. J. Janssen, M. Kemerink, *Nano Lett.* **2009**, *9*, 3032.
[10] C. Groves, O. G. Reid, D. S. Ginger, *Acc. Chem. Res.* **2010**, *43*, 612.
[11] T. Erb, U. Zhokhavets, G. Gobsch, S. Raleva, B. Stuhn, P. Schilinsky, C. Waldauf, C. J. Brabec, *Adv. Funct. Mater.* **2005**, *15*, 1193.
[12] X. N. Yang, J. Loos, S. C. Veenstra, W. J. H. Verhees, M. M. Wienk, J. M. Kroon, M. A. J. Michels, R. A. J. Janssen, *Nano Lett.* **2005**, *5*, 579.
[13] I. Arslan, T. J. V. Yates, N. D. Browning, P. A. Midgley, *Science* **2005**, *309*, 2195.
[14] S. van Bavel, E. Sourty, G. de With, K. Frolic, J. Loos, *Macromolecules* **2009**, *42*, 7396.
[15] S. van Bavel, E. Sourty, G. de With, S. Veenstra, J. Loos, *J. Mater. Chem.* **2009**, *19*, 5388.
[16] S. S. van Bavel, E. Sourty, G. de With, J. Loos, *Chin. J. Polym. Sci.* **2009**, *27*, 85.
[17] S. S. van Bavel, E. Sourty, G. de With, J. Loos, *Nano Lett.* **2009**, *9*, 507.
[18] A. A. Herzing, L. J. Richter, I. M. Anderson, *J. Phys. Chem. C* **2010**, *114*, 17501.
[19] S. D. Oosterhout, M. M. Wienk, S. S. van Bavel, R. Thiedmann, L. J. A. Koster, J. Gilot, J. Loos, V. Schmidt, R. A. J. Janssen, *Nat. Mater.* **2009**, *8*, 818.
[20] D. R. Kozub, K. Vakhshouri, L. M. Orme, C. Wang, A. Hexemer, E. D. Gomez, *Macromolecules* **2011**, *44*, 5722.

[21] R. B. Ross, C. M. Cardona, D. M. Guldi, S. G. Sankaranarayanan, M. O. Reese, N. Kopidakis, J. Peet, B. Walker, G. C. Bazan, E. van Keuren, B. C. Holloway, M. Drees, *Nat. Mater.* **2009**, *8*, 208.
[22] R. B. Ross, C. M. Cardona, F. B. Swain, D. M. Guldi, S. G. Sankaranarayanan, E. van Keuren, B. C. Holloway, M. Drees, *Adv. Funct. Mater.* **2009**, *19*, 2332.
[23] J. C. Hindson, Z. Saghi, J. C. Hernandez-Garrido, P. A. Midgley, N. C. Greenham, *Nano Lett.* **2011**, *11*, 904.
[24] J. Loos, E. Sourty, K. Lu, G. de With, S. van Bavel, *Macromolecules* **2009**, *42*, 2581.
[25] K. J. Batenburg, J. Sijbers, *IEEE Trans. Image Process.* **2011**, *20*, 2542.
[26] S. Bals, K. J. Batenburg, J. Verbeeck, J. Sijbers, G. Van Tendeloo, *Nano Lett.* **2007**, *7*, 3669.
[27] K. J. Batenburg, S. Bals, J. Sijbers, C. Kuebel, P. A. Midgley, J. C. Hernandez, U. Kaiser, E. R. Encina, E. A. Coronado, G. Van Tendeloo, *Ultramicroscopy* **2009**, *109*, 730.
[28] B. A. Collins, Z. Li, C. R. McNeill, H. Ade, *Macromolecules* **2011**, *44*, 9747.
[29] N. D. Treat, M. A. Brady, G. Smith, M. F. Toney, E. J. Kramer, C. J. Hawker, M. L. Chabinyc, *Adv. Energy Mater.* **2011**, *1*, 82.
[30] M. Pfannmöller, H. Flügge, G. Benner, I. Wacker, C. Sommer, M. Hanselmann, S. Schmale, H. Schmidt, F. A. Hamprecht, T. Rabe, W. Kowalsky, R. R. Schröder, *Nano Lett.* **2011**, *11*, 3099.
[31] B. A. Collins, E. Gann, L. Guignard, X. He, C. R. McNeill, H. Ade, *J. Phys. Chem. Lett.* **2010**, *1*, 3160.
[32] M. A. Ruderer, R. Meier, L. Porcar, R. Cubitt, P. Mueller-Buschbaum, *J. Phys. Chem. Lett.* **2012**, *3*, 683.
[33] H. Chen, R. Hegde, J. Browning, M. D. Dadmun, *Phys. Chem. Chem. Phys.* **2012**, *14*, 5635.
[34] A. Moulé, J. Bonekamp, K. Meerholz, *J. Appl. Phys.* **2006**, *100*, 094503.
[35] C. Müller, T. A. M. Ferenczi, M. Campoy-Quiles, J. M. Frost, D. D. C. Bradley, P. Smith, N. Stingelin-Stutzmann, J. Nelson, *Adv. Mater.* **2008**, *20*, 3510.
[36] J. Zhao, A. Swinnen, G. Van Assche, J. Manca, D. Vanderzande, B. Van Mele, *J. Phys. Chem. B* **2009**, *113*, 1587.
[37] M. Liedtke, A. Sperlich, H. Kraus, A. Baumann, C. Deibel, M. J. M. Wirix, J. Loos, C. M. Cardona, V. Dyakonov, *J. Amer. Chem. Soc.* **2011**, *133*, 9088.
[38] R. B. Ross, *Ph.D. Thesis,* Georgetown University, Washington D.C. **2009**.
[39] E. Busby, C. W. Rochester, A. J. Moulé, D. S. Larsen, *Chem. Phys. Lett.* **2011**, *513*, 77.
[40] F. Padinger, R. S. Rittberger, N. S. Sariciftci, *Adv. Funct. Mater.* **2003**, *13*, 85.
[41] L. M. Chen, Z. R. Hong, G. Li, Y. Yang, *Adv. Mater.* **2009**, *21*, 1434.
[42] A. J. Moulé, K. Meerholz, *Adv. Funct. Mater.* **2009**, *19*, 3028.
[43] A. C. Mayer, M. F. Toney, S. R. Scully, J. Rivnay, C. J. Brabec, M. Scharber, M. Koppe, M. Heeney, I. McCulloch, M. D. McGehee, *Adv. Funct. Mater.* **2009**, *19*, 1173.
[44] A. Moulé, A. Tsami, T. W. Brunnagel, M. Forster, N. M. Kronenberg, M. Scharber, M. Koppe, M. Morana, C. J. Brabec, K. Meerholz, U. Scherf, *Chem. Mater.* **2008**, *20*, 4045.
[45] S. A. Mauger, L. Chang, S. Friedrich, C. W. Rochester, D. M. Huang, P. Wang, A. J. Moulé, *Adv. Funct. Mater.* **2012**, DOI: 10.1002/adfm.201201874.
[46] G. Li, V. Shrotriya, Y. Yao, J. S. Huang, Y. Yang, *J. Mater. Chem.* **2007**, *17*, 3126.
[47] V. D. Mihailetchi, H. X. Xie, B. de Boer, L. J. A. Koster, P. W. M. Blom, *Adv. Funct. Mater.* **2006**, *16*, 699.
[48] V. D. Mihailetchi, H. X. Xie, B. de Boer, L. M. Popescu, J. C. Hummelen, P. W. M. Blom, L. J. A. Koster, *Appl. Phys. Lett.* **2006**, *89*, 012107.
[49] S. T. Turner, P. Pingel, R. Steyrleuthner, E. J. W. Crossland, S. Ludwigs, D. Neher, *Adv. Funct. Mater.* **2011**, *21*, 4640.
[50] Y. Gao, T. P. Martin, E. T. Niles, A. J. Wise, A. K. Thomas, J. K. Grey, *J. Phys. Chem. C* **2010**, *114*, 15121.
[51] W. R. Wu, U. S. Jeng, C. J. Su, K. H. Wei, M. S. Su, M. Y. Chiu, C. Y. Chen, W. B. Su, C. H. Su, A. C. Su, *ACS Nano* **2011**, *5*, 6233.
[52] D. Chen, A. Nakahara, D. Wei, D. Nordlund, T. P. Russell, *Nano Lett.* **2011**, *11*, 561.
[53] H. Hoppe, T. Glatzel, M. Niggemann, W. Schwinger, F. Schaeffler, A. Hinsch, M. C. Lux-Steiner, N. S. Sariciftci, *Thin Solid Films* **2006**, *511*, 587.
[54] L. Chang, H. W. A. Lademann, J. B. Bonekamp, K. Meerholz, A. J. Moulé, *Adv. Funct. Mater.* **2011**, *21*, 1779.
[55] E. Verploegen, R. Mondal, C. J. Bettinger, S. Sok, M. F. Toney, Z. Bao, *Adv. Funct. Mater.* **2010**, *20*, 3519.
[56] C. Z. Li, S. C. Chien, H. L. Yip, C. C. Chueh, F. C. Chen, Y. Matsuo, E. Nakamura, A. K. Y. Jen, *Chem. Comm.* **2011**, *47*, 10082.